Advances in Concrete Construction, *Vol. 16, No. 4 (2023) 217-230*
https://doi.org/10.12989/acc.2023.16.4.217

Prediction behavior of the concentric post-tensioned anchorage zones

Shangda Chen [1] and Linyun Zhou*[2]

[1] *School of Civil Engineering, Changchun University of Architecture and Civil Engineering, Changchun, Jilin, 130607, China*
[2] *School of Science, Nanjing University of Science and Technology, Nanjing 210096, China*

(*Received April 24, 2022, Revised December 26, 2023, Accepted April 17, 2024*)

Abstract. Methods for designing the post-tensioned anchorage zones at ultimate limit state has been specified in current design codes based on strut-and-tie models (STM). However, it is still not clear how to estimate the serviceability behavior of the anchorage zones. The serviceability is just indirectly taken into account by means of the reasonable reinforcement detailing. To address this issue, this paper is devoted to developing a modified strut-and-tie model (MSTM) to predict the behavior of concentric anchorage zones throughout the loading process. The principle of stationary complementary energy is introduced into STM at each load step to satisfy the compatibility condition and generate the unique MSTM. The structural behavior of anchorage zones can be achieved based on MSTM from loading to failure. Simplified formulas have been proposed to estimate the first cracking load, bearing capacity and maximum crack width with the consideration of the details of reinforcement bursting bars. The proposed model provides a definite method to control the bursting crack width in concentric anchorage zones. Four specimens with different bearing plate ratios have been designed and tested to validate the proposed method.

Keywords: maximum crack width; modified strut-and-tie model; post-tensioned anchorage zones; serviceability behavior

1. Introduction

The anchorage zone is defined as the portion of structure in which the concentrated post-tensioning forces is transferred from the anchorage device to the structure. It can be divided in two separate zones, that is, the local and the general zone (Breen *et al*. 1994). The local zone mainly bears local prestress forces and many models had been built to estimate the bearing capacity (Cervenka and Ganz 2014, Park *et al*. 2020, Rebelo *et al*. 2021). While the behavior of anchorage zones at ultimate limit state (ULS) is predicted based on the stress distribution at the linear elastic stage (KRTA 2010, AASHTO 2014, ACI 318-19 2019).

In the past decades, considerable efforts had been made on predicting the stresses distribution and ultimate capacity of anchorage zones (Steensels *et al*. 2017, Geng *et al*. 2019, Tan *et al*. 2020). By assuming that the reinforced concrete of anchorage zones is a homogenous, isotropic and elastic material, Guyon (1953) solved the transverse bursting stresses using fourier series, and proposed the compression dispersion model (CDM) to determine the bursting stresses distribution. Following the concept of CDM, Sahoo *et al*. (2009), He and Liu (2011) and Zhou *et al*. (2015) developed modified models to reproduce the distribution of the bursting stresses and correspondingly busting forces in concentric anchorage zones. Kim and Kim (2017) analyzed the stress magnitudes and distributions of rectangular post-tensioned anchorage zones using ultra-high performance concrete (UHPC), and they stated that UHPC can bear the bursting forces and significantly reduce the anchorage zone size. Based on three-dimensional linear elastic finite element analysis with design parameters, Kim *et al*. (2019) proposed the modified design equations to evaluate the bursting force in an anchorage block with rectangular anchorage plates and circular anchorage plates. In order to study the efficiency of the confinement reinforcement in anchorage zones of posttensioning tendons using high-performance fiber reinforced concrete, Marchão *et al*. (2019) conducted eleven prismatic anchorage zones and they found that the outer reinforcement is not as effective as the inner one, which leads to too high estimated load capacity. Moreover, HPFRC anchorage zones can reduce amount of confining reinforcement. To evaluate the compression stresses in concentric anchorage zones with special anchorage device, Park *et al*. (2020) developed an improved equation by considering the effect of the duct holes on the stress distribution. Based on the experiment investigation of ten post tensioned anchorage zones with high strength strands, Ro *et al*. (2020) stated that the ACI 318-19 and AASHTO standards were inadequate to calculate bearing force of post-tensioned members using high-strength strands. Furthermore, the anchorage reinforcement designed using current codes could not resist additional stress in the anchorage zone occurred as the flexural load increased.

As a consistent design approach for structural concrete, strut and tie model (STM) has been usually adopted to predict the ultimate capacity of concentric anchorage zones (Hou *et al*. 2017). However, STM developed based on the lower bound theorem of plasticity does not satisfy the compatibility conditions, which cannot be used to estimate the serviceability of structural concrete. Therefore, how to

*Corresponding author, Ph.D., Associate Professor,
E-mail: 21105309@163.com

ISSN: 2287-5301 (Print), 2287-531X (Online)

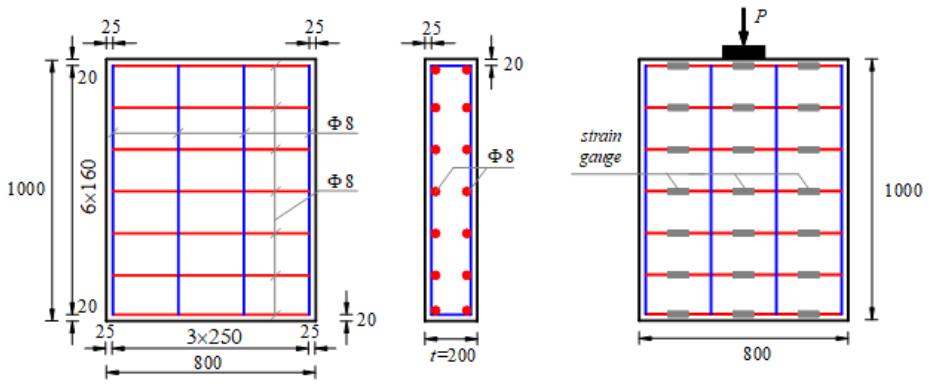

(a) Front view (b) side view (c) Arrangement of strain gauge

Fig. 1 Details of the specimens (dimension: mm)

predict the service behavior based on STM is one of the pressing problems in civil engineering (ASCE-ACI Committee 445 1998). Up till now, very few studies have addressed the service behavior after cracking (Lourenço and Almeida 2013, Zhou *et al*. 2017). In 2011, Lourenço and Almeida (2013) introduced the principle of minimum complementary energy into stress field model, and proposed a computer-based model to estimate the serviceability behavior of structural concrete. However, compared with the test results, the proposed model will overestimate the crack width. Based on the principle of the stationary complementary energy, Zhou *et al*. (2017) proposed the elastic-to-plastic STM (EPSTM) to predict the service behavior of anchorage zones. However, there are two unreasonable aspects in EPSTM for concentric anchorage zones. First, the test results show that the busting forces balanced by the upper tie is 1.02 times that of lower tie at ULS, while in EPSTM the ratio of the bursting forces in upper tie and lower tie is 0.83, which conflicted with the test results. Second, after cracking the configuration parameters of STM will be governed by the details of the reinforcement bars. That is, it is irrational to predict the bearing capacity and serviceability behavior of anchorage zones without the consideration of details of reinforcement bars.

To advance the STM for satisfying the compatibility conditions, this study aims to develop a new rational model, modified STM (MSTM), to predict the behavior of post-tensioned anchorage zones throughout the loading process.

2. Experimental program

2.1 Test specimens

According to the design codes AASHTO (2014), four test specimens with different bearing plate ratios were designed to investigate the service behavior of post-tensioned anchorage zones as shown in Fig. 1. The length and height of the specimens were 1.0 m and 0.8 m, respectively. The thickness of the specimens are t = 0.2 m. Rectangular bearing plate with the width of 0.2 m are placed on the center of the anchorage zones. The bearing plate ratios (areas rations of the bearing plates and

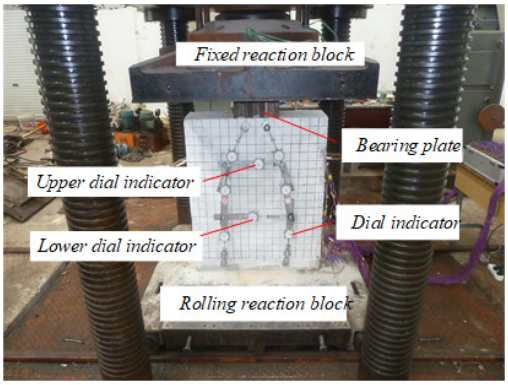

Fig. 2 Test setup of the concentric anchorage zones

specimens) were set to be 0.1, 0.2, 0.3 and 0.375 for the specimen S1, S2, S3 and S4, respectively. Concrete cover (0.02 m) and spacing (0.16 m) between reinforcement bars were chosen according to the code provisions. The diameter of the reinforcement bars was 8 mm. Based on the material tests, the modulus of elasticity and compressive strength of concrete were tested to be $E_c = 3.45 \times 10^4$MPa and $f_c' =$ 38.6 MPa, respectively. And the yield stress of reinforcement bar was $f_{ys} = 525$ MPa.

Concentric load was applied on the top of the specimens to model the anchor forces as shown in Fig. 2. All of the test specimens were monotonically loaded over the full thickness so that the specimens would behave in two dimensions. Concrete surface cracks were located by visual observation, and the monitoring of strain gauge data was placed on the key reinforcement as shown in Fig. 1(c). Dial gauges were placed on key locations to measure the deformation, average compressive strain and tensile strain of reinforced struts and ties throughout the loading process. Two dial indicators were used to monitor the average tensile strain of the ties, the upper dial indicator placed at the centroid of the second layer steel and third layer steel, and the lower dial indicator placed at the centroid of the other bursting bars.

2.2 Test results and Analysis

For all specimens, test events progressed very similarly

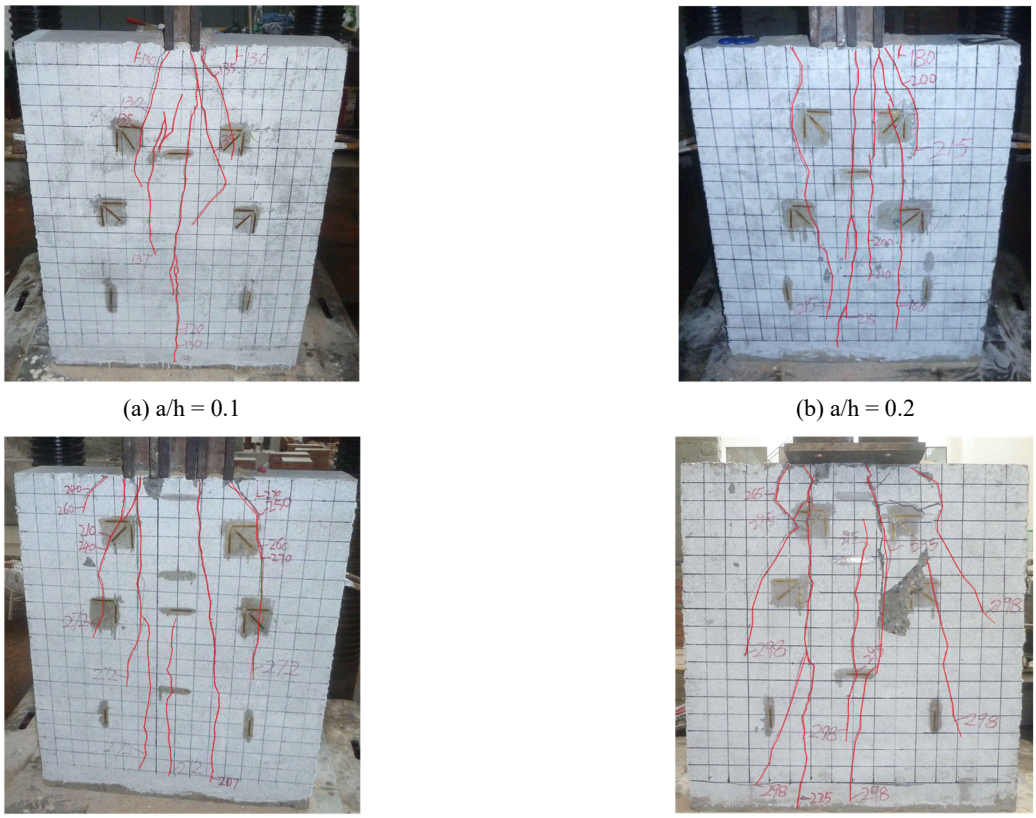

(a) a/h = 0.1 (b) a/h = 0.2

(c) a/h = 0.3 (d) a/h = 0.375

Fig. 3 Crack pattern at failure load: (a) for A1; (b) for A2; (c) for A3; and (d) for A4

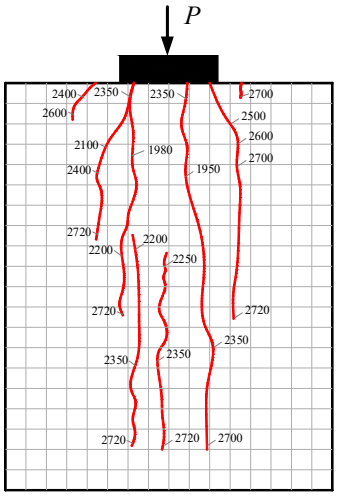

Fig. 4 Crack pattern for the anchorage zone with a/h = 0.3

as indicated in Fig. 3. As for the specimen S3 (the bearing ratio a/h is 0.3), the first bursting crack, with a length of 45 cm, initiated for a load of 1950 kN. As expected the bursting crack located close to the maximum elastic bursting stress along the centerline. It also shall be noted that the location of the bursting crack was shifted from the centerline due to the heterogeneity of matrix properties. Another bursting crack occurred at the symmetrical position for a load of 1980 kN as shown in Fig. 4. The bursting cracks propagated over the thickness of the section and propagated towards the loading face and away from it substantially. Spalling cracks, 12.5 cm from the centerline of the specimen, were observed when the load reached 2400 kN. With the increment of load, a diagonal crack occurred along the edge of the bearing plate on the left hand side. When the load was 2350 kN, the busting crack propagated to load face, meanwhile the vertical strain measured by the dial gauges indicated that the bars reached the yield strain, and the corresponding diagonal crack width was 0.37 mm. Due to the existence and growth of the bursting cracks, the position of the resultant forces at the far-end section gradually moved towards the centerline of specimen. Throughout the loading process, the maximum crack width, gradually increased with the load. Moreover, it should be noted that, as stated by Gergely and Sozen (1967), the length of bursting crack increases significantly faster than the crack width in the single concentric anchorage zone.

Fig. 5 shows the average strain of reinforcement steel of the test specimen with different bearing ratios. It can be seen that the stress in the reinforcement steel A was compressive stress before cracking. After cracking, the stress decreased rapidly due to the crack growth, and eventually changed into tensile stress. The other bursting reinforcement bars bear tensile stresses in the loading process. The steel stresses increased rapidly due to the crack growth and stress redistribution after cracking. At ULS, the strain of the second layer steel reached the yield strain, and the strain of the third layer steel was very close to the yield strain. While the strains of the other bars were less than the yield strain and gradually decreased with the distance

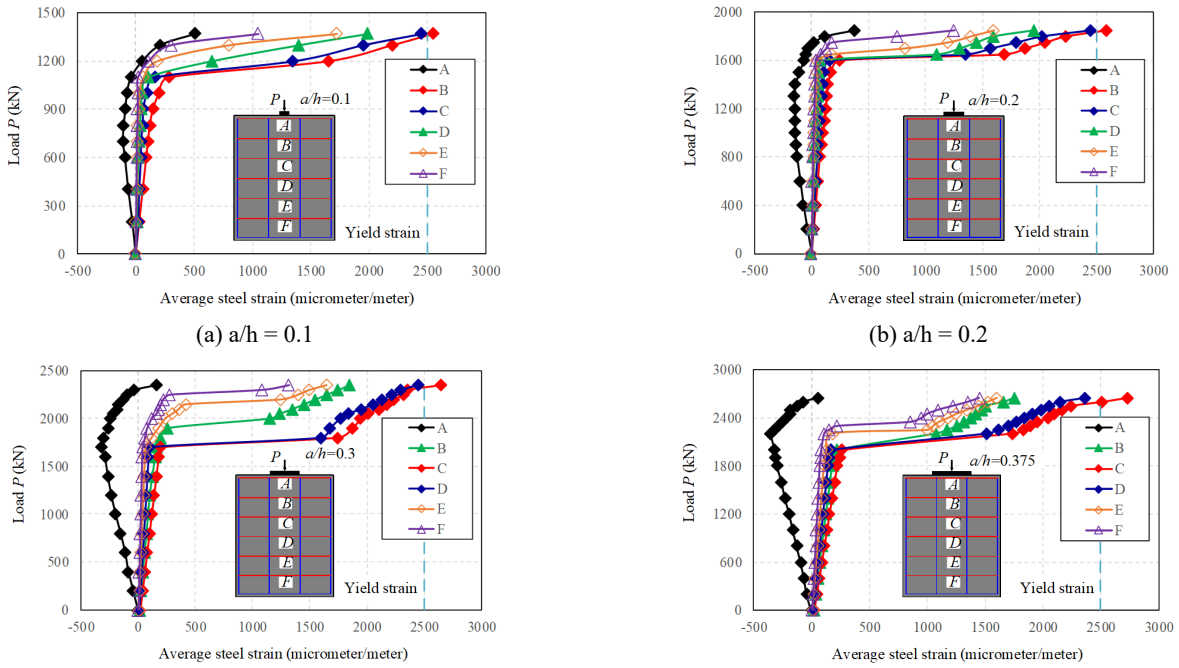

(a) a/h = 0.1 (b) a/h = 0.2

(c) a/h = 0.3 (d) a/h = 0.375

Fig. 5 Average bursting steel strain of the test specimens

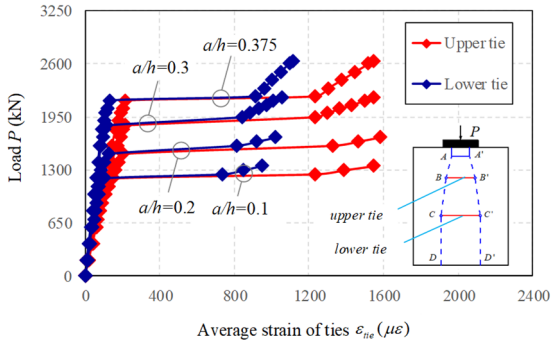

Fig. 6 Average strain of the ties

between bars and loading plate. It indicates that the strain of the reinforcement bars increased significantly when the cracks crossed the bursting steel, that is, the ties will gradually move towards the far end section of the anchorage zones. More in detail, the experimental curves are characterized by two to three changes in its slope, corresponding to the cracking behavior (bursting crack, spalling crack and diagonal crack) in the loading process.

The upper dial indicator and lower dial indicator are used to measure the average strain of the ties in anchorage zone. Thus, two ties were defined in the test specimens based on the location of the dial indicator, that is, upper tie and lower tie. Fig. 6 shows the measured strain of the upper tie and lower tie in anchorage zone. It can be seen that the upper tie and lower tie behave similar to the bursting steel. At failure, the average strain of the upper tie was $1600\ \mu\varepsilon$ for all specimens, and the strain of lower tie were $948\ \mu\varepsilon$, $1020\ \mu\varepsilon$, $1055\ \mu\varepsilon$ and $1120\ \mu\varepsilon$ for specimen S1, S2, S3 and S4, respectively. That is the ratios of the transverse bursting forces balanced by upper tie and lower were was 1.12, 1.04, 1.01 and 0.95 at ULS.

The whole structural response of the test specimens, including the first cracking load, capacity, average strain of steel, load-deformation curve and the maximum crack width, will be discussed in the following section.

3. Development of MSTM

3.1 Compatibility conditions in MSTM

According to the principle of the stationary complementary energy, among all the admissible stress fields, the function of the complementary energy is rendered stationary only by actual stress fields which satisfy compatibility and the displacement boundary conditions. Thus, the compatibility conditions can be satisfied for STM when the function of the complementary energy is rendered stationary.

To satisfy the compatibility, the configuration of the MSTM shall be adjusted with the external load P. Let's assume that the adjusted configuration parameters are X_i, then the principle of minimum complementary energy can be expressed by

$$\frac{\partial B(P, X_i)}{\partial X_i} = 0 \tag{1}$$

in which, B is the complementary energy of ties and struts.

By solving the above equation, the configuration of STM can be determined by each load step, and the corresponding structural behavior can be achieved. In contrast to the traditional STM, the MSTM allows a consistent analysis of the behavior of structural concrete throughout the loading process.

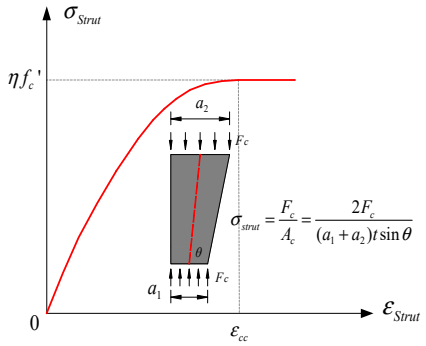

Fig. 7 Idealized stress-strain curve for concrete struts

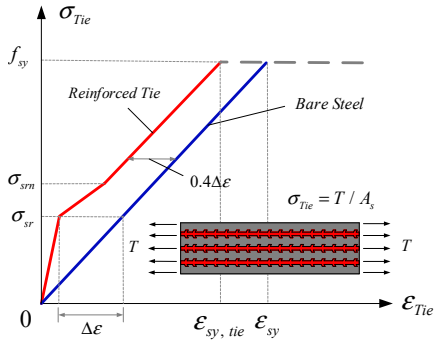

Fig. 8 Idealized behavior of a reinforced tie

3.2 Complementary energy of struts and ties

In post tensioned anchorage zones, the concrete struts are assumed to be prismatic shape and the compressive stress uniformly distributed across the effective width, that is, the average compressive stress can be obtained by simply dividing the axial force by the strut area, then the strain of the struts can be determined based on the constitutive laws of concrete struts as shown in Fig. 7. The stress-strain curve for the struts follows the average curve obtained from concrete test cylinders

$$\sigma_{strut} = \eta f_c' \left(\frac{2\varepsilon_i}{\varepsilon_{cc}} - \frac{{\varepsilon_i}^2}{{\varepsilon_{cc}}^2} \right) \tag{2}$$

in which, σ_{strut} and ε_i are the average stress and strain of the struts; f_c' is the cylinder compressive strength of concrete; $\varepsilon_{cc} = -0.002$ s the strain at peak compressive stress; η represents the reduction of concrete strength (Vecchio and Collins 1986).

Ties are composed of reinforcing steel and surrounding concrete. Following the Model Code (2010), Fig. 8 illustrates the idealized stress-strain relationship for the reinforced ties. As for the uncracked stage, the stress-stain relationship of ties behaves linearly and can be expressed by

$$\varepsilon_{tie} = \frac{n\rho\sigma_{tie}}{E_s(1+n\rho)} \tag{3}$$

in which, $n = E_s/E_c$ is modular ratio; $\rho = A_s/A_c$ is the geometrical ratio of reinforcement;

For the crack formation phase, the average strain of tension chord can be given by

$$\varepsilon_{tie} = \frac{\sigma_{tie}}{E_s} - \frac{3\sigma_{sr} - 2\sigma_{tie}}{\sigma_{sr}}\Delta\varepsilon \tag{4}$$

where $\sigma_{sr} = f_{ct}(1+n\rho)/\rho$ is the steel stresses at cracks; and $\Delta\varepsilon = \lambda f_{ct}(1/\rho - 1)/E_s$ is the increase of steel strain in the cracking state.

For stabilized cracking phase, the ties behave linearly again and the average stain can be expressed by

$$\varepsilon_{tie} = \frac{\sigma_{tie}}{E_s} - 0.4\Delta\varepsilon \tag{5}$$

By Integrating the average stresses over the average stain, the complementary energy of the struts (or ties) can be given by

$$\Delta B_i = \int_0^{\sigma} \varepsilon_i d\sigma_i \tag{6}$$

Thus, the total complementary energy in MSTM can be given by

$$B = \sum A_i l_i \Delta B_i \tag{7}$$

where A_i and l_i are the area and length of the struts (or ties), respectively.

4. Behavior of anchorage zones

4.1 MSTM for anchorage zones

Fig. 9 illustrates the load transfer path and geometric definition of the concrete struts in the post tensioned anchorage zones. Although multi layers of reinforcement bars are placed in the real structure, two admissible ties are enough to describe the load transfer mechanism in the post-tensioned anchorage zones. According to the test results, the strain of second layer steel and third layer steel are very close and much more than the others, that is, the upper tie can be assumed to locate at the centroid of the second

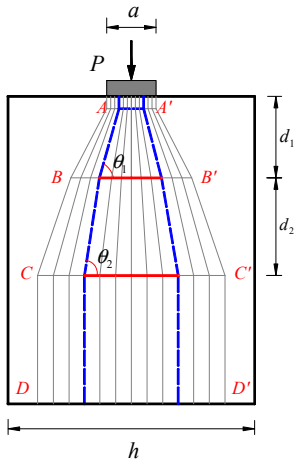

Fig. 9 Geometric definition of the concrete struts

Table 1 Geometric dimension and forces in the struts and ties

Members	Length l_i	Force F_i	Area A_i
AB	$\frac{d_1 - a/4}{\sin\theta_1}$	$\frac{P}{2\sin\theta_1}$	$\left(\frac{d_1-\frac{a}{4}}{\tan\theta_1}+\frac{a}{2}\right)t\sin\theta_1$
BC	$\frac{d_2}{\sin\theta_2}$	$\frac{P}{2\sin\theta_2}$	$\left(\frac{d_2}{\tan\theta_2}+\frac{2d_1-\frac{a}{2}}{\tan\theta_1}+\frac{a}{2}\right)t\sin\theta_2$
CD	$h-d_1-d_2$	$\frac{P}{2}$	$\left(\frac{2d_2}{\tan\theta_2}+\frac{2d_1-\frac{a}{2}}{\tan\theta_1}+\frac{a}{2}\right)t$
CC'	$\frac{2d_2}{\tan\theta_2}+\frac{2d_1-a/2}{\tan\theta_1}+\frac{a}{2}$	$\frac{P}{2\tan\theta_2}$	A_{s2}
BB'	$\frac{2d_1-a/2}{\tan\theta_1}+\frac{a}{2}$	$\frac{P}{2}\left(\frac{1}{\tan\theta_1}-\frac{1}{\tan\theta_2}\right)$	A_{s1}

layer steel and third layer steel ($d_1 = 26$ cm). The lower tie is composed of the other bursting bars, and the distance between the two ties is assumed to be d_2. Then, a preliminary configuration of STM with unknown parameters, θ_1, θ_2 and d_2, can be developed, where the blue dashed line represents the struts, and the red solid line represents ties. It shall be noted that due to the stress redistribution after cracking, the configuration of MSTM will change with the external loads. Thus, Node B and B' can move freely in the in the horizontal direction; while Node C and C' can move freely in the horizontal direction and vertical direction with the load.

According to the MSTM, the forces in the struts and ties can be calculated based on the equilibrium condition at load P as listed in Table 1, where a is the bearing plate width; t is the thickness of the anchorage zones; and A_{s1}, A_{s2} are the cross-sectional areas of upper and lower ties, respectively. Therefore, the complementary energy in the struts, B_c, and ties, B_s, can be presented by

$$\begin{aligned} B_c &= \sum A_{ci} l_{ci} \Delta B_{ci} \\ &= 2\sum (A_{cAB} l_{cAB} \Delta B_{cAB} + A_{cBC} l_{cBC} \Delta B_{cBC} \\ &\quad + A_{cCD} l_{cCD} \Delta B_{cCD}) \end{aligned} \tag{8a}$$

$$\begin{aligned} B_s &= \sum A_{si} l_{si} \Delta B_{si} \\ &= \sum (A_{sBB'} l_{sBB'} \Delta B_{sBB'} + A_{sCC'} l_{sCC'} \Delta B_{sCC'}) \end{aligned} \tag{8b}$$

Thus, the govern differential equations of MSTM can be given by

$$\frac{\partial (B_c + B_s)}{\partial \theta_1} = 0 \tag{9a}$$

$$\frac{\partial (B_c + B_s)}{\partial \theta_2} = 0 \tag{9b}$$

$$\frac{\partial (B_c + B_s)}{\partial d_2} = 0 \tag{9c}$$

It is hard to obtain an analytical solution for each configuration parameter because of the coupling of the govern equations. Computer code is presented to solve the above equations and determine the configuration of MSTM at each load step. Then, following the equilibrium condition and constitutive laws for ties and struts, the structural behavior of anchorage zones throughout the loading process can be achieved.

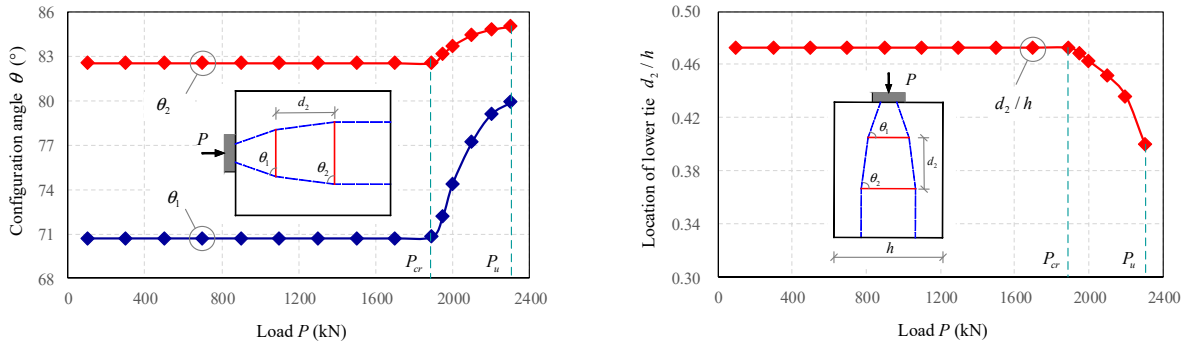

Fig. 10 Adaptive configuration parameters of MSTM throughout the loading process for test specimen S3: (a) configuration angles; and (b) location of the lower tie

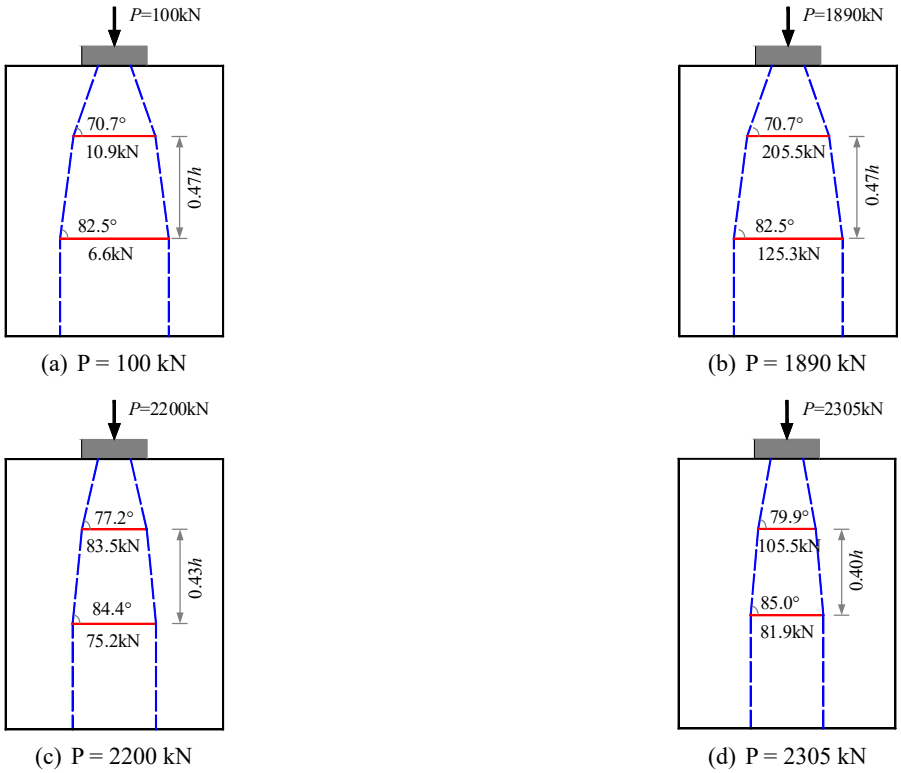

(a) P = 100 kN (b) P = 1890 kN

(c) P = 2200 kN (d) P = 2305 kN

Fig. 11 MSTM of the concentric anchorage zone with a/h = 0.3: (a) elastic stage P = 100 kN; (b) first cracking load P = 1890 kN; (c) P = 2200 kN; (d) ultimate load P = 2305 kN

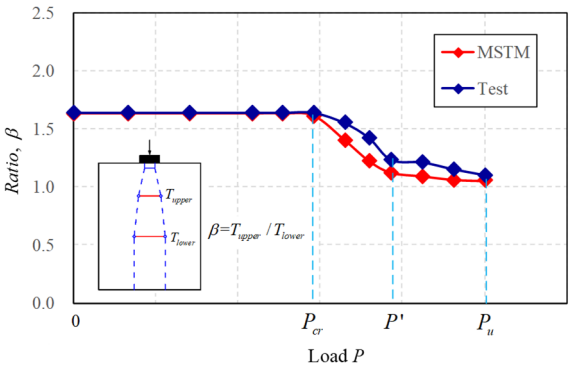

Fig. 12 Ratio of the bursting forces balanced by the upper tie and lower tie throughout the loading process

4.2 Load resistance mechanism

According to the layout of reinforcement and geometrical dimensions of the test specimens S3 (a/h = 0.3), Fig. 10 shows the configuration parameters of the MSTM calculated by Eq. (9) throughout the loading process, and the corresponding MSTM at each load steps is illustrated in Fig. 11. It can be seen that prior to cracking, θ_1 and θ_2 always remain the same, which mainly depend on the distribution of the busting stresses in elastic stage. After cracking, the forces in the ties will decrease suddenly as illustrated in Fig. 11(c) because the cracked concrete cannot bear transverse busting forces. Meanwhile the average strain of the ties increases rapidly and the stain of the upper tie is much larger than that of lower tie. As a result, the lower tie will move towards the upper tie to make its strain close to the strain of upper tie. Moreover, θ_1 and θ_2 will gradually increase with the load, and the increase ratio of θ_2 is slightly larger than θ_1 as described in Fig. 10. At ULS, the upper tie reaches its ultimate capacity, whereas, the upper tie is not yield.

Fig. 12 shows the ratios of the bursting forces resisted by the upper tie and lower tie β. As can be seen, in elastic stage the bursting forces in MSTM is approximately equal to 0.18 P, and the contribution of upper tie is 0.11 P. The ratio β is $\beta_c = 1.62$ and keep constant till cracking as shown in Fig. 12, which coincides with the test results. After cracking ($P > P_{cr}$), the contribution of the concrete for the bursting forces decrease sharply, and the average strain of the ties increases suddenly due to the stress redistribution, which leads to crack propagation. There is an inflection point on the ratio curve at $P = P'$, it means that the bursting cracks cross the fifth layer of steel. When the load approaches its maximum value, the upper tie reaches its ultimate capacity ($T = f_{ys}A_{s1} = 105.5$ kN) as shown in Fig. 11(d). It is very interesting that the value of β at ULS is $\beta_u = 1.02$, which agrees with the test of results as stated before.

4.3 First cracking load

Based on the equilibrium conditions in MSTM and the ratio of β in the elastic stage, the tensile forces in the upper tie can be given by

$$T_{1c} = \frac{\beta_0}{1+\beta_0}\frac{P(1-\gamma)}{4} \tag{10}$$

Table 2 Predictions of the first cracking load of concentric anchorage zones

Specimen	a/h	t (m)	f_c' (MPa)	Test $P_{cr,T}$ (kN)	Predictions/Test		
					MSTM	Eq. (12)	Eq. (13)
S1	0.10	0.2	38.6	1250	1.01	1.56	0.76
S2	0.2	0.2	38.6	1550	0.95	1.39	0.69
S3	0.3	0.2	38.6	1950	0.97	1.40	0.62
S4	0.375	0.2	38.6	2200	0.96	1.43	0.62
B1	0.06	0.1	21.8	160	0.95	1.25	0.87
B2	0.06	0.1	26.6	165	0.96	1.93	0.83
B3	0.06	0.1	26.6	178	0.98	1.48	1.27
B4	0.06	0.1	26.6	196	1.01	1.62	1.16
B5	0.06	0.1	19.7	178	1.02	1.17	1.04
B6	0.06	0.1	19.7	242	0.94	1.15	0.76
B7	0.06	0.1	19.7	178	0.96	1.38	0.62
B8	0.06	0.1	30.8	334	0.92	1.76	0.75
B9	0.06	0.2	30.8	445	0.97	1.83	0.79
B10	0.06	0.2	29.8	476	0.93	1.79	0.72
B11	0.06	0.1	17.0	142	0.96	1.01	0.70
B12	0.06	0.1	24.4	245	0.95	1.39	0.87
R1	0.25	0.1	44.9	550	1.02	1.33	0.59
R2	0.13	0.1	39.2	250	0.92	1.52	0.84
R3	0.13	0.1	44.9	300	0.94	1.71	0.77
R4	0.06	0.1	39.2	225	0.93	1.67	0.87
R5	0.06	0.1	42.3	180	0.92	1.72	1.14
Mean					0.96	1.51	0.82
Standard deviation					0.03	0.24	0.19

where $\beta_0 = 1.62$ is the ratio of the bursting forces resisted by upper tie and lower tie before cracking; P is the external load; and γ is the bearing plate ratio.

Following the constitutive laws of the ties, the first crack will occur when the stress in the upper tie reaches the tensile strength of reinforced tie. That is, the first cracking load, P_{cr}, of the concentric anchorage zones can be derived by

$$P_{cr} = \frac{2A_{s1}f_{ct}\left(n+\frac{1}{\rho}\right)}{\left(\frac{1}{tan\,\theta_{1c}}-\frac{1}{tan\,\theta_{2c}}\right)} = \frac{2(1+\beta_c)A_{s1}f_{ct}(n+1/\rho)}{\beta_c(1-\gamma)} \quad (11)$$

in which, A_{s1} is the area of the bursting bars in upper tie; f_{ct} is the tensile strength of concrete; $n = E_s/E_c$ is the modular ratio; and $\rho = A_s/(st)$ is the geometrical ratio of reinforcement, where s is the reinforcement spacing; t is the thickness of the specimen.

Eqs. (12) and (13) shows the predicted first cracking load for anchorage zones proposed by Stone and Breen (1984) and He and Liu (2011), respectively.

$$P_{cr} = \left[\frac{tf_t\text{'}}{24}(38h-120)-7t\right]+39a+16f_t\text{'}-9 \quad (12)$$

$$P_{cr} = \frac{2ht}{1-\gamma}f_t\text{'} \quad (13)$$

in which, a is the width of bearing plate; f_t' is the split cylinder tensile strength and can be conservatively estimated by $f_t\text{'} = 0.214(f_c\text{'})^{0.69}$ (Oluokun 1991).

Table 2 lists the first cracking load obtained by MSTM, Eq. (12) and Eq. (13). Specimens B1–B12 were tested by Berezovytch (1970), and specimens R1-R4 were reported by Wong (1986). It can be seen that the predictions of MSTM agree well with the test results, the mean value of Prediction/Test are 0.96, 0.91 and 0.94, respectively. While the results of Eq. (12) are found to be a little conservative (with a mean Prediction/Test value of 0.82) due to ignorance of the contribution of the bursting bars. The equations proposed by Stone and Breen will overestimate the cracking loads with wide discreteness (the mean value of Prediction/Test is 1.5 and the standard deviation is 0.24).

4.4 Ultimate load

The test specimen indicates that the configuration of MSTM at ULS varies with the detail of reinforcement and bearing plate ratio. To investigate the behavior of anchorage zones at ULS, a parameter analysis is conducted. The dimensions of the anchorage zones are set to be same with

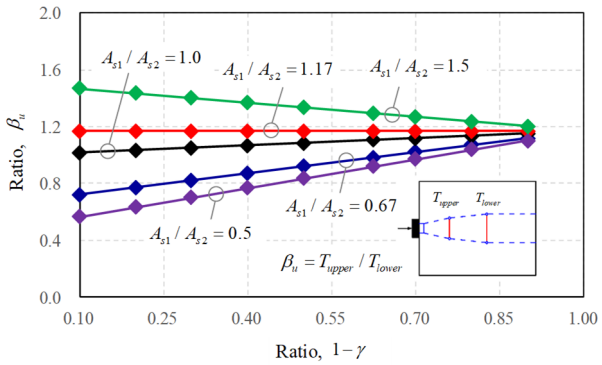

Fig. 13 Ratio of the bursting forces balanced by the upper tie and lower tie at ULS with different bearing plate ratios

the test specimen. Fig. 13 shows the ratio of the bursting forces resisted by the upper tie and lower tie (β_u) with different bearing plate ratios (γ) area ratios of ties ($A_{s1}/A_{s2} = 1.17$) at ULS, in which A_{s1} and A_{s2} are the areas of the upper tie and lower tie, respectively. It can be seen that when $A_{s1}/A_{s2} = 1.17$, β_u keeps constant $\beta_u = 1.17$ with different γ, which indicates that the upper tie and lower tie will reach the yield stress simultaneously. When the area ratio is less than 1.17, the ratio of β_u will increase linearly with the bearing plate ratios, and the maximum limit value is 1.17, which means that the upper tie will reach the yield stress at ULS, while the strain of the lower tie will be less than the yield strain, and the bearing capacity will be governed by the strength of the upper tie. Fig. 14 shows the effect of bearing plate ratio (γ), bursting steel spacing (s) and location of the upper tie (d_1) on the location of the lower tie (d_2). It can be seen that d_2 increase linearly with s and d_1, and the bearing plate ratio have little effect on d_2; Moreover, d_2 gradually increases with the increment of ratio A_{s1}/A_{s2}. Fig. 15 shows the relationships between d_2 and θ_{2u} (the value of θ_2 at ULS) with different bearing plate ratios. As can be seen that the value of $d_2/h\tan\theta_{2u}$ decreases linearly with the increment of the ratio A_{s1}/A_{s2}, which indicates that the width of the struts paralleled to the anchor force decreases with A_{s1}/A_{s2}, as a result, the value of $d_2/h\tan\theta_{2u}$ will decrease rapidly as shown in Fig. 15.

According to Figs. 13, 14 and 15, the value of β_u, d_2 and θ_{2u} at ULS can be approximated by

$$\beta_u = \frac{T_{upper}}{T_{lower}} = \frac{A_{s1}}{A_{s2}} + \left(1.17 - \frac{A_{s1}}{A_{s2}}\right)(1-\gamma) \tag{14}$$

$$d_2 = \frac{3s}{4}\frac{A_{s1}}{A_{s2}} + \frac{d_1}{2} \tag{15}$$

$$\tan\theta_{2u} = \frac{2h}{\beta_u(1-\gamma)d_2} \tag{16}$$

where s is the bursting steel spacing; and d_1 is the location of the upper tie.

Then, the capacity of the upper tie (P_{upper}) and lower tie (P_{lower}) can be derived based on the geometric condition

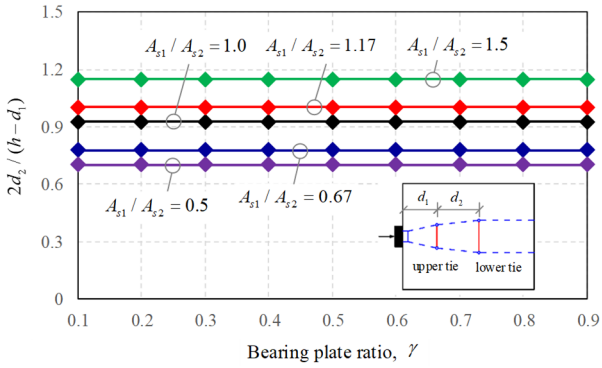

(a)

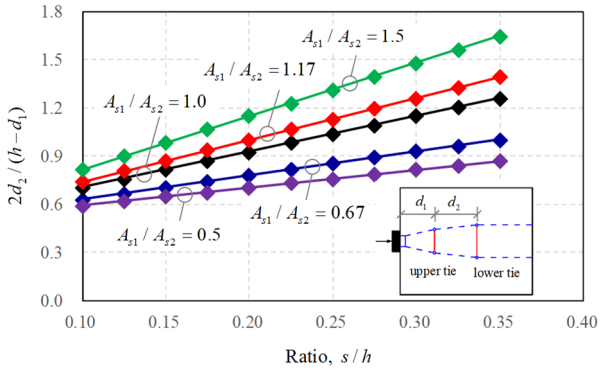

(b)

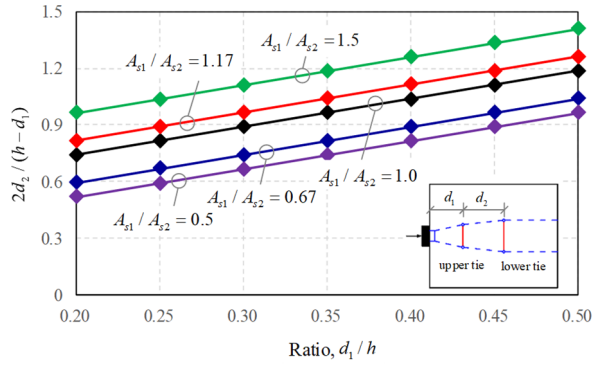

(c)

Fig. 14 Influence of the details of anchorage zones on the location of the lower tie; (a) Bearing plate ratio; (b) Stirrup spacing and (c) location of the upper tie

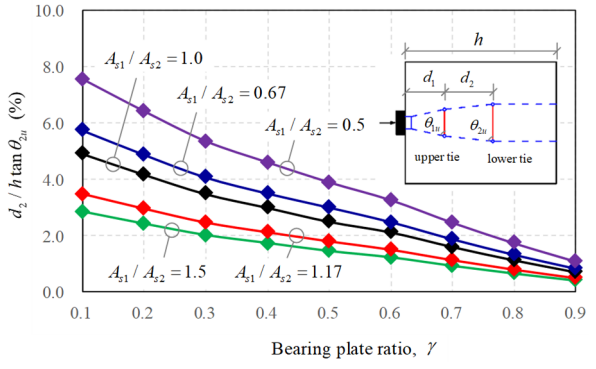

Fig. 15 Relationships between d_2 and θ_{2u} at ULS of anchorage zones with different bearing plate ratios

Table 3 Comparisons between predicted and experimental ultimate load

Specimen	a/h	t (m)	f_c' (MPa)	Test $P_{u,T}$ (kN)	Predictions/Test		
					MSTM	ACI (Model Code)	PTI
S1	0.10	0.2	38.6	1250	1.01	1.56	0.76
S2	0.2	0.2	38.6	1550	0.95	1.39	0.69
S3	0.3	0.2	38.6	1950	0.97	1.40	0.62
S4	0.375	0.2	38.6	2200	0.96	1.43	0.62
B1	0.06	0.1	21.8	160	0.95	1.25	0.87
B2	0.06	0.1	26.6	165	0.96	1.93	0.83
B3	0.06	0.1	26.6	178	0.98	1.48	1.27
B4	0.06	0.1	26.6	196	1.01	1.62	1.16
B5	0.06	0.1	19.7	178	1.02	1.17	1.04
B6	0.06	0.1	19.7	242	0.94	1.15	0.76
B7	0.06	0.1	19.7	178	0.96	1.38	0.62
B8	0.06	0.1	30.8	334	0.92	1.76	0.75
B9	0.06	0.2	30.8	445	0.97	1.83	0.79
B10	0.06	0.2	29.8	476	0.93	1.79	0.72
B11	0.06	0.1	17.0	142	0.96	1.01	0.70
B12	0.06	0.1	24.4	245	0.95	1.39	0.87
R1	0.25	0.1	44.9	550	1.02	1.33	0.59
R2	0.13	0.1	39.2	250	0.92	1.52	0.84
R3	0.13	0.1	44.9	300	0.94	1.71	0.77
R4	0.06	0.1	39.2	225	0.93	1.67	0.87
R5	0.06	0.1	42.3	180	0.92	1.72	1.14
Mean					0.96	1.51	0.82
Standard deviation					0.03	0.24	0.19

$$P_{upper} = \frac{2}{\beta_u} A_{s1} f_{ys} \tan\theta_{2u} = \frac{4hA_{s1}f_{ys}}{{\beta_u}^2(1-\gamma)d_2} \quad (17)$$

$$P_{lower} = \frac{4hA_{s2}f_{ys}}{\beta_u(1-\gamma)d_2} \quad (18)$$

Therefore, the ultimate load of concentric anchorage zones can be obtained by

$$P_u = min\ (P_{upper}, P_{lower}) \quad (19)$$

where $A_{s1}f_{ys}$ and $A_{s2}f_{ys}$ are the capacity of the bursting steel in the upper tie and lower tie, respectively. It also shall be noted that this section mainly discus the bearing capacity governed by ties, and the failures of nodes and concrete struts are not included.

In current design codes, including ACI 318-19 (2019), PTI (2000) and Model Code (2010), based on the assumption that all the bursting bars reach the yield strain at ULS, the bearing capacity can be derived by the transverse bursting forces. Table 3 lists the capacity of anchorage zones predicted by EPSTM and current design codes, in which specimens A1-A4, B1-B6 and R1-R4 were tested by Sanders and Breen (1997), Breen *et al*. (1994) and Wong (1986), respectively. It can be seen that MSTM produces a good agreement with the test results, the average Prediction/ Test value is 0.96 and the standard deviation is 0.02; while ACI 318-19 and Model Code give a conservative result in most cases due to without the consideration of stress redistribution after cracking, the mean value of Prediction/ Test is just 0.79. PTI will overly underestimate the capacity of the anchorage zones because the unreasonable predicted bursting forces.

4.5 Average strain of bursting steel

By solving Eq. (9) at each load step, the configuration parameters of MSTM can be determined, and the forces in the ties and struts can be derived based on the equilibrium conditions. Then according to constitutive laws of struts and reinforced ties as illustrated in Figs. 7 and 8, the strain-load response of concrete, bursting steel, struts and ties can be estimated. Fig. 16 shows the average strain of the bursting steel in the upper tie and lower tie predicted by MSTM. It can be seen that before cracking, the bursting reinforcement bars behave linearly with the anchor force, and the predictions agree well with the test results, the maximum deviation is 6.2%, 7.6%, 4.3% and 7.1% for specimen S1, S2, S3 and S4, respectively. After cracking, the average steel strains increase sharply because the bursting forces are assumed to be only resisted by the bursting steel. Thereafter, the average steel strain approximately increases

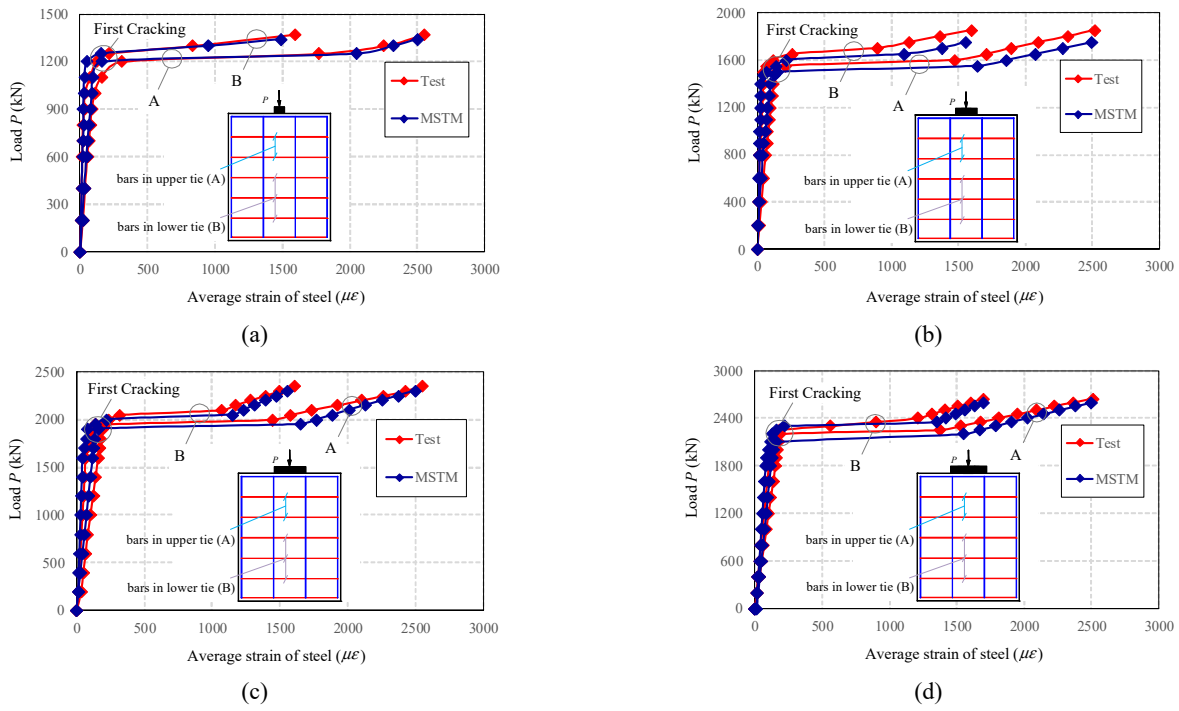

Fig. 16 Average strain of reinforcement bars in ties for anchorage zones with different bearing plate ratios: (a) a/h = 0.1; (b) a/h = 0.2; (3) a/h = 0.3 and (d) a/h = 0.375

linearly with the load. The predictions are slightly larger than the test results because the constitutive laws of ties are developed based on the pure tension chord, without the consideration of shear stresses and lateral stresses in the loading process. Moreover, the diagonal cracks and spalling cracks are not considered in MSTM. The ratios of the average strain of the reinforcement bars in the upper tie and lower tie at ULS are 1.68, 1.61, 1.53 and 1.47 for specimen S1, S2, S3 and S4, respectively. And the corresponding ratios β_u are 1.12, 1.07, 1.02 and 0.98 for specimen S1, S2, S3 and S4, respectively, which is coincident with the test results. In general, the predictions have a good agreement with the test results.

4.6 Load-deformation response

According to the principle of conservative energy in MSTM, the deformation of the anchorage zones, Δ, can be derived by

$$\Delta = \frac{2\sum F_i L_i \varepsilon_i}{P} \tag{20}$$

in which, P is the external load; F_i, L_i and ε_i is the force, length and average strain of the struts or ties, respectively.

Fig. 17 plots the predicted deformation of anchorage zones with different bearing plate ratios. It can be seen that before cracking, the predictions are slightly less than the test results, because the transverse bursting stresses at the far end section is not zero, as a result, the total strain energy of MSTM will be less than in reality. While after cracking, the predictions are slightly larger than the test results due to without the consideration of the diagonal cracks and

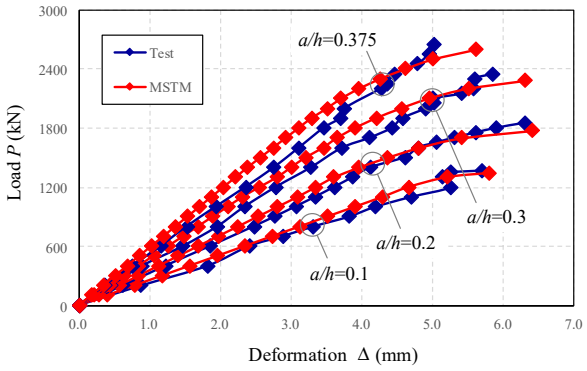

Fig. 17 Load-deformation curves for the test specimens

spalling cracks. The maximum relative deviations are 4.2%, 6.8%, 5.7% and 5.3% for the test specimen S1, S2, S3 and S4, respectively. In general, the MSTM can provide a reasonable estimate of the overall load-deformation response of the test anchorage zones.

4.7 Maximum crack width

In a cracked tension chord the strain incompatibility is accommodated by the relative displacement between steel and concrete. Assumed that there is only one crack in the ties, thus the crack width can be given by

$$w = \int_{l_{cr}} (\varepsilon_s - \varepsilon_c) dx = l_{cr} \varepsilon_{tie} \tag{21}$$

in which ε_s and ε_c are the average stain of steel and concrete respectively; ε_{tie} is the average strain of the

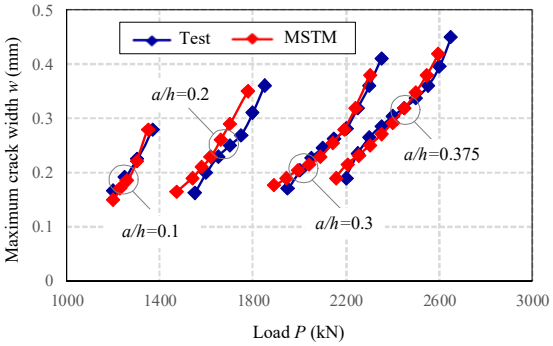

Fig. 18 Maximum crack width of the anchorage zones

reinforced tie and can be determined by MSTM; $l_{cr} = \phi_s \sigma_{sr}/(2\tau_b)$ is the crack spacing, where ϕ_s is the equivalent diameter of bundled bars; $\sigma_{sr} = f_{ct}(1+n\rho)/\rho$ is the steel stress at the crack as illustrated in Fig. 8; τ_b is the average bond stress and can be determined by Li *et al.* (2015)

$$\tau_b = 2.73\sqrt{f_c'} + 0.31\frac{p_1}{\sqrt{f_c'}} + 0.15\frac{p_2}{\sqrt{f_c'}} \quad (22)$$

in which, f_c' is the cylinder compressive strength of concrete; $p_1 = T_{upper}/A_{s1}$ and $p_2 = P/(2tl_{s1})$ are axial stress and lateral stress in the reinforced ties, respectively; t is thickness of the anchorage zones; T_{s1}, A_{s1} and l_{s1} are the tensile force, area and length of the upper tie, respectively.

Substituting Eq. (22) into Eq. (21), the maximum crack width in the reinforced tie, w_m, can be derived by

$$w = \frac{\sqrt{f_c'}\phi_s f_{ct}\varepsilon_{tie}(1+n\rho)/\rho}{(5.46f_c' + 0.62T_{upper}/A_{s1} + 0.3P/2tl_{s1})} \quad (23)$$

Fig. 18 compares the maximum crack width calculated by Eq. (23) and tests results. It can be seen that the maximum crack width increases rapidly with the increment of load, and then the increase ratio gradually decreases due to the occurrence of because the spalling cracks and diagonal cracks. At ULS, the maximum crack width of the concentric anchorage zones increases linearly with the bearing plate ratios. The calculated crack widths of the anchorage zones with different bearing plate ratios agree well with the test results. The maximum relative errors for specimen S1, S2, S3 and S4 are only 7.8, 5.7, 4.3, and 2.6%, respectively.

Following Eq. (23), the maximum crack width will be governed by the average strain of the upper tie ε_{tie} when the external load and mechanical properties of concrete. Meanwhile ε_{tie} will be dominated by the diameter of bursting steel, steel spacing, area ratios in upper tie and lower tie and so on. In other words, the crack width can be controlled through detailing the reinforcement bursting steel.

5. Conclusions

By introducing the compatibility conditions into STM, a modified STM (MSTM) is proposed to predict the structural behaviour of the post-tensioned anchorage zones throughout the loading process. Unique configuration of MSTM can be achieved by minimizing the complementary energy at each load step. The validation of the proposed MSTM has been verified by the test results. The following conclusions can be drawn:

- The proposed MSTM provides a consistent method to estimate the structural behaviour of concentric anchorage zones from loading to failure, and has been validated to be sufficiently accurate by the test results.
- Taking into account of the details of bursting steel, simplified formulas have been formed to predict the first cracking load and bearing capacity of the anchorage zones with suitable accuracy. The current design codes give a very conservative capacity due to not considering the stress redistribution and layout of reinforcement steel.
- A simplified method has been developed to assess the maximum bursting crack width in anchorage zones throughout the loading process. Moreover, it also provides an effective tool to control the crack width at service via detailing bursting steel.

Acknowledgments

This work was sponsored in part by 2023 Scientific research projects of the Education Department of Jilin Province of China (JJKH20231486KJ).

References

AASHTO (2014), AASHTO LRFD bridge design specifications, Washington, DC, USA.

ACI Committee 318 (2019), Building Code Requirements for Reinforced Concrete and Commentary, American Concrete Institute; Farmington Hills, MI, USA.

ASCE-ACI Committee 445 on Shear and Torsion (1998), "Recent approaches to shear design of structural concrete", *J. Struct. Eng.*, **24**, 1375-1417.

Berezovytch, W. (1970), "A study of the behavior of a single strand post-tensioning anchor in concrete slabs", Master Dissertation; The University of Texas at Austin, TX, USA.

Breen, J.E., Burdet, O., Roberts, C., Sanders, D. and Wollmann, G. (1994), "Anchorage zone reinforcement for post-tensioned concrete girders", National Cooperative Highway Research Program Report 356, Washington, DC, USA, 8-11.

Cervenka, V. and Ganz, H. (2014), "Validation of post-tensioning anchorage zones by laboratory testing and numerical simulation", *Struct. Concrete*, **15**(2), 258-268. https://doi.org/10.1002/suco.201300038

Geng, X., Zhou, W. and Yan, J. (2019), "Reinforcement of orthogonal ties in steel-fiber-reinforced reactive powder concrete anchorage zone", *Adv. Struct. Eng.*, **22**(10), 2311-2321. https://doi.org/10.1177/1369433219838085

Gergely, P. and Sozen, M.A. (1967), "Design of anchorage zone reinforcement in prestressed concrete beams", *PCI J.*, **12**(2), 63-

75.
Guyon, Y. (1953), *Prestressed Concrete*, John Wiley and Sons, New York, USA.
He, Z. and Liu, Z. (2011), "Investigation of bursting forces in anchorage zones: compression- dispersion models and unified design equation", *ASCE J. Bridge Eng.*, **16**(6), 820-827. https://doi.org/10.1061/(ASCE)BE.1943-5592.0000187
Hou, D., Zhao, J, Shen, L. and Chen, J. (2017), "Investigation and improvement of strut-and-tie model for design of end anchorage zone in post-tensioned concrete structure", *Constr. Build. Mater.*, **136**, 482-494. https://doi.org/10.1016/j.conbuildmat.2017.01.033
Kim, S. and Kim, T. (2017), "A stress analysis of the post-tensioned anchorage zones using UHPC", *Key Eng. Mater.*, **737**, 500-504. https://doi.org/10.4028/www.scientific.net/KEM.737.500
Kim, J., Kwak, H. and Kim, B. (2019), "Design equation to evaluate bursting forces at the end zone of post-tensioned members", *Comput. Concrete, Int. J.*, **24**(5), 423-436. https://doi.org/10.12989/cac.2019.24.5.423
Korea Road and Transportation Association (KRTA) (2010), *Design Code for Highway Bridges*, KRTA, Seoul, Republic of Korea.
Li, X., Wu, Z., Zheng, J. and Wei, D. (2015), "Effect of loading rate on the bond behavior of plain round bars in concrete under lateral pressure", *Constr. Build. Mater.*, **94**, 826-836. https://doi.org/10.1016/j.conbuildmat.2015.07.085
Lourenço, M. and Almeida, J. (2013), "Adaptive stress field models: formulation and validation", *ACI Struct. J.*, **110**, 71-81.
Marchão, C., Lucio, V. and Ganz, H. (2019), "Efficiency of the confinement reinforcement in anchorage zones of posttensioning tendons", *Struct. Concrete*, **20**(3), 1182-1198. https://doi.org/10.1002/suco.201800238
Model Code (2010), Final draft, fib – Bulletins 65 & 55, Fib; Lausanne, Switzerland.
Oluokun, F. (1991), "Prediction of concrete tensile strength from its compressive strength", *ACI Mater. J.*, **88**(3), 302-309. https://doi.org/10.14359/1942
Park, Y., Kim, M., Park, J. and Jeon, S. (2020), "An improved equation for predicting compressive stress in posttensioned anchorage zone", *Adv. Civil Eng.*, **2020**, 5635060. https://doi.org/10.1155/2020/5635060
Post-Tensioning Institute (2000), Anchorage Zone Design, Phoenix, AZ, USA.
Rebelo, J., Carla, M. and Lucio, V. (2021), "Study on the efficiency of confinement reinforcement in post-tensioning anchorage zones", *Magaz. Concrete Res.*, **73**(6), 271-287. https://doi.org/10.1680/jmacr.19.00050
Ro, K.M., Kim, M.S. and Lee, Y.H. (2020), "Validity of anchorage zone design for post tensioned concrete members with high-strength strands", *Appl. Sci.*, **10**(9), 3039. https://doi.org/10.3390/app10093039
Sahoo, D., Singh, D. and Bhargava, P. (2009), "Investigation of dispersion of compression in bottle-shaped struts", *ACI Struct. J.*, **2**, 178-186.
Sanders, D. and Breen, J. (1997), "Post-tensioned anchorage zones with single straight concentric anchorages", *ACI Struct. J.*, **2**, 146-158. https://doi.org/10.14359/469
Steensels, R., Vandewalle, L., Vandoren, B. and Degee, H. (2017), "A two-stage modelling approach for the analysis of the stress distribution in anchorage zones of pre-tensioned concrete elements", *Eng. Struct.*, **143**(15), 384-397. https://doi.org/10.1016/j.engstruct.2017.04.011
Stone, W., Filho, W. and Breen, J.E. (1984), "Behavior of post-tensioned girder anchorage zones", *PCI J.*, **29**(1), 64-109.
Tan, H., Zeng, Y. and Zhang, Q. (2020), "Optimization method of fatigue maintenance for cable-beam anchorage zone of suspension bridge", *Science Progress*, **103**, 1-12. https://doi.org/10.1177/0036850420950137
Vecchio, F.J. and Collins, M.P. (1986), "The modified compression field theory for reinforced concrete elements subjected to shear", *ACI Struct. J.*, **83**(2), 219-231.
Wong, K. (1986), "Shear strength and bearing capacity of reinforced concrete deep beams", Ph.D. Dissertation; The University of Leeds, UK.
Zhou, L., Liu, Z. and He, Z. (2015), "Further investigation of transverse stresses and bursting forces in post tensioned anchorage zones", *Struct. Concrete*, **16**, 84-92. https://doi.org/10.1002/suco.201400005
Zhou, L., Liu, Z. and He. Z. (2017), "Elastic-to-plastic strut and tie model for concentric anchorage zones", *J. Bridge Eng.*, **22**, 04017070. https://doi.org/10.1061/(ASCE)BE.1943-5592.0001060

Notations

a	length of bearing plate
$A_i,\ l_i$	area and length of the struts (or ties)
$A_{s1},\ A_{s2}$	areas of upper and lower ties
B	total complementary energy
$B_c,\ B_s$	complementary energy in the struts and ties
$d_1,\ d_2$	location of the upper tie and lower tie
$E_c,\ E_s$	elastic modulus of concrete and steel
$F_i,\ \varepsilon_i$	force and average strain of the struts or ties
l_{cr}	crack spacing
f_c'	compressive strength of concrete
f_{ct}	tensile strength of concrete
f_t'	split cylinder tensile strength of concrete
f_{ys}	yield stress of reinforcement bar
h	length of anchorage zones
$n = E_s/E_c$	modular ratio
P	external load
$P_{cr},\ P_u$	First cracking load and ultimate load
$p_1,\ p_2$	axial stress and lateral stress in the reinforced ties
s	reinforcement spacing
t	thickness of the anchorage zones
β	ratio of the bursting forces resisted by the upper tie and lower tie
β_0	ratio of the bursting forces resisted by upper tie and lower tie before cracking
β_u	ratio of the bursting forces resisted by upper tie and lower tie at ULS
γ	bearing plate ratio
$\theta_1,\ \theta_2$	angle between the struts and upper tie or lower tie
$\varepsilon_s,\ \varepsilon_c$	average stain of steel and concrete
$\varepsilon_{strut},\ \varepsilon_{tie}$	average strain of the struts and ties
ρ	geometrical ratio of reinforcement
$\sigma_{strut},\ \sigma_{tie}$	average stress of the struts and ties
σ_{sr}	steel stresses at cracks
τ_b	average bond stress
ϕ_s	equivalent diameter of bundled bars